Cerium Oxide Nanoclusters on Graphene/Ru(0001): Intercalation of Oxygen *via* Spillover

Zbynek Novotny,[†] Falko P. Netzer,[*,‡] and Zdenek Dohnálek[*,†]

[†]Fundamental and Computational Sciences Directorate and Institute for Interfacial Catalysis, Pacific Northwest National Laboratory, Richland, Washington 99354, United States and [‡]Surface and Interface Physics, Institute of Physics, Karl-Franzens University, A-8010 Graz, Austria

ABSTRACT Cerium oxide is an important catalytic material known for its ability to store and release oxygen, and as such, it has been used in a range of applications, both as an active catalyst and as a catalyst support. Using scanning tunneling microscopy and Auger electron spectroscopy, we investigated oxygen interactions with CeO_x nanoclusters on a complete graphene monolayer-covered Ru(0001) surface at elevated temperatures (600−725 K). Under oxidizing conditions ($P_{O_2} = 1 \times 10^{-7}$ Torr), oxygen intercalation under the graphene layer is observed. Time dependent studies demonstrate that the intercalation proceeds *via* spillover of oxygen from CeO_x nanoclusters through the graphene (Gr) layer onto the Ru(0001) substrate and extends until the Gr layer is completely intercalated. Atomically resolved images further show that oxygen forms a $p(2 \times 1)$ structure underneath the Gr monolayer. Temperature dependent studies yield an apparent kinetic barrier for the intercalation of 1.21 eV. This value correlates well with the theoretically determined value for the reduction of small CeO_2 clusters reported previously. At higher temperatures, the intercalation is followed by a slower etching of the intercalated graphene (apparent barrier of 1.60 eV). Vacuum annealing of the intercalated Gr leads to the formation of carbon monoxide, causing etching of the graphene film, demonstrating that the spillover of oxygen is not reversible. In agreement with previous studies, no intercalation is observed on a complete graphene monolayer without CeO_x clusters, even in the presence of a large number of point defects. These studies demonstrate that the easily reducible CeO_x clusters act as intercalation gateways capable of efficiently delivering oxygen underneath the graphene layer.

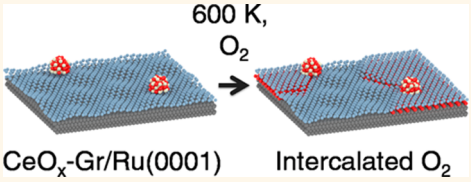

KEYWORDS: ceria · oxide cluster · graphene on Ru · scanning tunneling microscopy · Auger electron spectroscopy · graphene etching · oxygen intercalation · spillover

Cerium oxide is a catalyst material of high importance because of its wide range of applications. It has an exceptionally high oxygen storage-release capacity (OSRC), and thus can be easily reduced and oxidized. Consequently, ceria plays an important role in many redox reactions. The reduction of ceria and the release of oxygen is linked to the creation of an oxygen vacancy (V_O) and the formation of a pair of Ce^{3+} ions.[1] When the V_O is refilled, the pair of Ce^{3+} changes back to the 4+ charge state. Ceria has been extensively examined both theoretically and experimentally, and has been the subject of a number of review articles.[2,3]

While most of the mechanistic insights (like V_O formation)[4] were gained from studies of the most stable, least reactive (111) surface under ultra-high vacuum (UHV) conditions,[2] it was soon established that in redox processes, ceria nanoparticles are much more reactive than atomically flat, low-index single crystal surfaces. The reactivity of ceria nanoparticles exhibits a size dependency, with a maximum reactivity reported for nanoparticles having size between 2 and 3 nm.[5]

To study the redox properties of ceria nanoparticles using surface science techniques, a suitable support is needed. Metal surfaces are suitable but active substrates, and are known to initiate spillover of oxygen from ceria to the metal.[6−9] On the other hand, carbon-based supports are inert and present ideal substrates because of their high thermal and chemical stability. We have chosen a supported graphene (Gr) layer[10] as a two-dimensional model of the practically more important carbon nanotube systems.[11,12] As a support metal for Gr, we have selected the Ru(0001) surface, because Gr/Ru(0001) is one of the most investigated supported Gr systems with a known structure,[13] and a large number of theoretical and experimental studies exist,[14−28] including those addressing the interaction

* Address correspondence to falko.netzer@uni-graz.at, zdenek.dohnalek@pnnl.gov.

Received for review June 30, 2015 and accepted July 31, 2015.

Published online July 31, 2015
10.1021/acsnano.5b03987

© 2015 American Chemical Society

with oxygen.[22−28] These latter studies were typically performed on Gr partially covering the metal substrate, and oxygen was found to be able to intercalate between Gr and the metal substrate. The mechanism of intercalation for Gr/Ru(0001) slightly differs from other supported Gr systems because of a different Gr−substrate bond strength,[25,27] but all previously reported supported Gr systems share a common property: intercalation of oxygen requires areas of the exposed bare metal surface for dissociation of oxygen molecules,[29] followed by diffusion of atomic oxygen underneath the Gr film.[22,24−26,28] Perfectly closed Gr layers without any metallic/metal-oxide ad species are reportedly able to protect the supporting metal against oxidation, both in high vacuum studies at high temperature,[27,30] or at near-ambient pressure conditions at room temperature (RT).[28] Only at high temperatures (above 700 K) under oxygen-rich conditions can Gr be etched away.[31] Therefore, at moderate temperatures (up to ~700 K), a complete layer of supported Gr should be an ideal substrate to study the redox properties of ceria nanoclusters.

We have studied the interaction of ceria nanoclusters deposited on Gr/Ru(0001) with molecular oxygen at temperatures between 600 and 725 K using scanning tunneling microscopy (STM) and Auger electron spectroscopy (AES). Surprisingly, we found that at elevated temperatures in a reactive oxygen atmosphere ($P_{O_2} = 1 \times 10^{-7}$ Torr), CeO_x clusters can facilitate intercalation of oxygen underneath the Gr layer. Due the presence of CeO_x clusters, the intercalation of oxygen progresses at a rapid rate compared to the situation without the CeO_x clusters, where holes in the protective Gr film have to be etched first. In contrast with previous studies, the CeO_x clusters allow for the intercalation of a full Gr monolayer without its etching. We propose that in the presence of CeO_x clusters, oxygen is delivered underneath Gr *via* spillover from CeO_x clusters through subnanometer size holes that have opened up in Gr underneath the CeO_x clusters. The reverse spillover of oxygen is not observed, and annealing of the intercalated Gr in vacuum leads to the formation of carbon monoxide, resulting from the reactive etching of the graphene film. This CeO_x-Gr/Ru(0001) represents a model catalytic system with an exceptionally high OSRC, since the amount of oxygen stored is not only determined by the capacity of the ceria nanoparticles, but a much larger amount of oxygen can be stored underneath the Gr.

RESULTS AND DISCUSSION

Preparation of CeO_x Clusters. For Gr preparation (detailed in the Methods section), we used very similar growth conditions as described in ref 28, resulting in a single-layer Gr fully covering the Ru(0001) substrate. Multilayer Gr[32,33] or exposed Ru areas were never observed in our STM images. Figure 1a shows this single layer Gr/Ru(0001) after the deposition of 0.05 monolayer of Ce (ML, 1 ML ≡ 1.24×10^{15} Ce/cm^2) in 1×10^{-7} Torr O_2 background at room temperature (RT, ~300 K). The inset in Figure 1a shows a zoom-in image into an area with a clean Gr surface with no CeO_x clusters present. Gr/Ru(0001) forms a Moiré structure with a large corrugation,[14] caused by the strong interaction of Gr with the supporting Ru(0001) substrate.[15] The interaction strength varies across the Moiré, from weakly bound where Gr hexagons are centered on top of the underlying Ru sites (imaged bright, inset of Figure 1a) to strongly bound regions centered on top the hollow-site (dark in STM). A unit cell consisting of (25 × 25) Gr on (23 × 23) Ru cells is highlighted in the image.[13]

After a small amount of Ce is deposited in 1×10^{-7} Torr O_2 on Gr/Ru(0001) at RT, clusters with an average diameter of ~3 nm and height of 1−2 ML (based on the O−Ce−O repeating unit along the [111] direction with a height of 3.12 Å) are observed. The density of CeO_x clusters determined from STM images is $(2.98 \pm 0.15) \times 10^{11}$ clusters/cm^2, with ~80% of nanoparticles having an apparent height of 1 ML following deposition at RT. Using the total Ce deposited amount of 6.2×10^{13} Ce/cm^2, we estimate that each cluster contains on average ~200 Ce atoms. The nucleation sites of these clusters are ascribed to defects in the Gr overlayer (see Figure S1a, Supporting Information). Significant spatial variations in local defect densities are observed in STM images. This is especially prominent during etching of Gr, because etching is known to start at defects.[24] As STM can probe only a very small area, the images are not always truly representative of the entire surface. This highlights the necessity of using surface averaging spectroscopic techniques, like AES or X-ray photoelectron spectroscopy for further characterization. The surface represented in Figure 1a (0.05 ML CeO_x−Gr/Ru(0001)) represents the starting point for all experiments presented in this article. We varied the temperature and exposure time to oxygen, monitoring the changes of the surface with STM and AES at RT. We used STM to image the structure of the surface, and AES allowed us to monitor the fractional Gr coverage and the amount of intercalated oxygen. Because of the small amount of Ce metal deposited, we could not use AES to determine the stoichiometry of the CeO_x clusters (Ce features are below the detection limit, see Figure S2). Mullins *et al.*[34] have shown that fully oxidized ceria films can be grown using oxygen pressures near 10^{-7} Torr, using nearly the same deposition rate as used here. Consequently, the ceria clusters should have a near-stoichiometric composition after the deposition.

Evolution of Surface Structure and Morphology During Oxygen Intercalation. The interaction of CeO_x clusters supported on Gr/Ru(0001) with oxygen at a fixed temperature of 641 K has been followed by STM. Both heating and cooling were performed in molecular oxygen. After 20 min of annealing, most of the surface is still covered with bare Gr (Figure 1b), but in areas

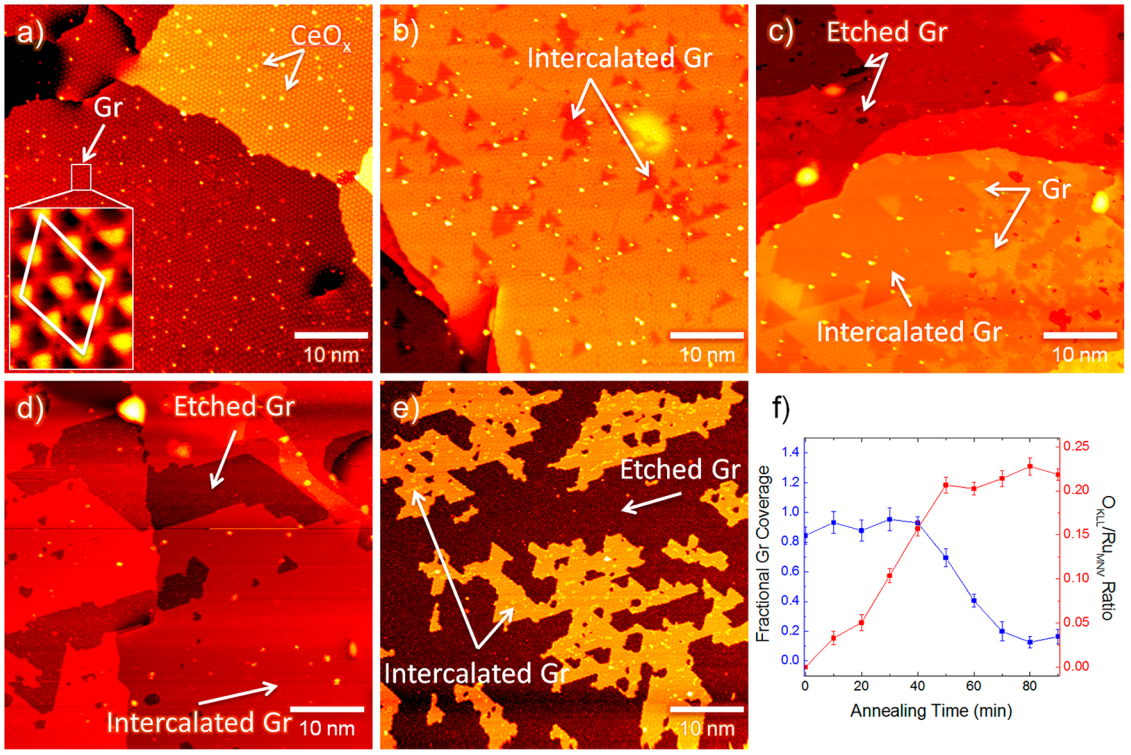

Figure 1. CeO_x mediated intercalation of oxygen underneath Gr/Ru(0001), monitored with STM (a−e) and AES (f). (a) A 0.05 ML CeO_x deposited onto Gr/Ru(0001) at RT. Initially, Gr Moiré and CeO_x clusters are observed. Inset in (a) shows a highlighted Gr supercell with 2 × 2 crystallographically inequivalent Gr subcells. Annealing the surface shown in (a) at 641 K in 1×10^{-7} Torr O_2 for 20 min (b) results in the intercalation of oxygen next to CeO_x clusters. After 40 min of O_2 annealing (c), most of the Gr is intercalated, and an onset of Gr etching is observed. Later, at 60 min (d), Gr is fully intercalated, with a few etched areas observed. Finally, after 80 min (e), most of the Gr is etched away, while the remaining Gr flakes are fully intercalated with oxygen. Panel f shows the fractional coverage of Gr and the amount of intercalated oxygen as a function of annealing time at 641 K in 1×10^{-7} Torr O_2. STM scanning conditions: $V_{sample} = -(1.5-1.6)$ V, $I_{tunnel} = 25-100$ pA.

bordering to the CeO_x clusters a dramatic decrease of the amplitude of corrugation of the Gr Moiré is noted. Atomically resolved images (Figure 2a,b) show that these areas are consistent with intercalated oxygen, as reported previously on Gr flakes.[23,24,28,31] In addition, sintering[35] of the CeO_x clusters also occurred.

The intercalation proceeds with additional annealing in oxygen (40 min, Figure 1c). We observe further sintering of the CeO_x clusters, together with the formation of larger clusters stabilized at screw dislocations and step edges and the onset of Gr etching. After annealing for 60 min (Figure 1d), Gr is completely intercalated with no pristine areas observable in the STM images. Also, a significant etching of Gr is recognized. Continued annealing in oxygen (80 min, Figure 1e) etches away most of the Gr film, with the remaining Gr flakes being fully intercalated. Low-energy electron diffraction (LEED) diagrams taken from the surfaces shown in Figure 1b−e reveal the appearance of half-integer spots, originating from a structure with either $p(2 \times 2)$ or $p(2 \times 1)$ symmetry (data not shown); these two structures cannot be distinguished by means of qualitative LEED observations.[36]

In addition to STM, the intercalation process has been monitored by AES (Figure 1f): the fractional coverage of Gr and the amount of surface oxygen has been followed. The coverage of Gr was estimated from the ratio of the negative to positive excursions of the 272−273 eV derivative AES peak (representing the overlapping C_{KLL} and Ru_{MNN} transitions), where we utilized the asymmetry of the graphitic carbon signal in AES, as compared to the relatively symmetric Ru_{MNN} peak[37,38] (see Figure S2). The uncertainty of this procedure leads to an additional error that is estimated to be ∼10% in addition to the error bars shown. The $p(2 \times 2)$−O/Ru(0001) and 0.05 ML CeO_x−Gr/Ru(0001) surfaces were used as reference spectra (Figure S2) to determine the full Gr coverage. The oxygen signal is plotted as the ratio of the O_{KLL} (510 eV) to Ru_{MNV} (231 eV) peaks, since the latter is not affected by the presence of graphitic carbon on the surface.[38] AES results are in a good agreement with the STM measurements: for the first 40 min of annealing in O_2, the fractional Gr coverage remains unchanged, while the uptake of the O_{KLL}/Ru_{MNV} ratio indicates the presence of intercalated oxygen underneath Gr. With O_{KLL}/Ru_{MNV} reaching saturation value ($t > 40$ min), the rate of Gr etching accelerates. In agreement with previous studies, the etching proceeds faster on intercalated Gr than on nonintercalated Gr.[25]

In Figure 2, zoom-in images of the important features observed in the large-scale images in Figure 1 are

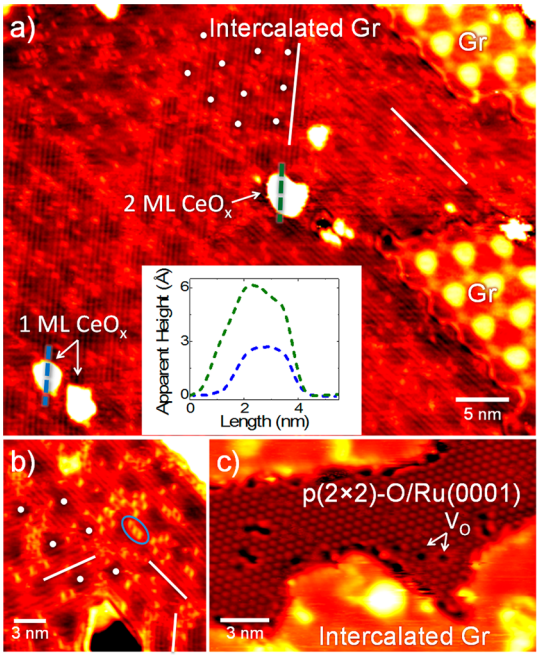

Figure 2. Atomically resolved STM images of oxygen-intercalated Gr and etched Gr areas: 0.05 ML CeO_x−Gr/Ru(0001) annealed at 641 K in 1×10^{-7} Torr O_2 for 40 min (a and b) and 80 min (c). Panel a shows an atomically resolved image with CeO_x clusters; the contrast of the clusters has been oversaturated in order to enhance the contrast of intercalated Gr area. Gr symmetry in the intercalated area is emphasized with white dots; the orientation of the intercalated $p(2 \times 1)$−O domains is highlighted with white lines. Line profile (dashed blue line) over the smallest 1 ML cluster and (dashed green line) for 2 ML cluster is shown in the inset. Panel b is a zoom-in image of a different intercalated area, showing all three possible $p(2 \times 1)$−O domains within one intercalated area (domain orientations are highlighted with white lines). The bright protrusions (three of them highlighted with a blue ellipse), highly mobile at RT, presumably originate from trapped gas molecules underneath Gr. (c) Etched Gr area with a $p(2 \times 2)$−O structure; V_O designates a couple of oxygen vacancies. STM scanning conditions: $V_{sample} = -1.6$ V, $I_{tunnel} = 25-100$ pA.

presented. In panel a, intercalated Gr extends over most of the image, with two nonintercalated Gr areas in the right part of the image. The corrugation amplitude of the intercalated Gr Moiré is largely reduced,[23,24] although still visible (highlighted by white dots). Note that the contrast of the CeO_x clusters is oversaturated with the brightness settings used here. The intercalated oxygen forms rows of atoms, with a row separation of 5.4 Å. To image the subsurface region, we utilized the fact that for specific tip compositions,[39] and after scanning for a certain time at high bias voltage, Gr can become "transparent".[40] Two different orientations of intercalated oxygen rows are observed in Figure 2a, rotated 120° with respect to each other (direction of rows is highlighted with white lines). This structure is consistent with the $p(2 \times 1)$−O reconstruction observed on the clean Ru(0001) surface.[29] Figure 2b shows another example of intercalated Gr with all three possible orientations of oxygen rows (indicated by white lines). Furthermore, bright protrusions located between intercalated oxygen rows are seen (three of them are emphasized by the blue ellipse in Figure 2b). Time-lapsed STM images show a high mobility of these features at RT (data not shown). These features are ascribed to trapped gas molecules, possibly CO or CO_2.[41] The $p(2 \times 1)$ structure for oxygen-intercalated areas was reported previously by LEED−$I(V)$ measurements,[24] and, indirectly, by a change of contrast in low-energy electron microscopy images,[25] caused by the different work function of $p(2 \times 2)$-O and $p(2 \times 1)$−O reconstructions on Ru(0001).[36] Here, we provide real space STM images, confirming the $p(2 \times 1)$−O saturation coverage of intercalated oxygen underneath Gr. The second process observed during annealing Gr with CeO_x clusters in oxygen at 641 K was the etching of Gr. A zoom-in image into one of the etched areas is displayed in Figure 2c. The etched areas show a $p(2 \times 2)$ symmetry, consistent with the $p(2 \times 2)$−O reconstruction of the Ru(0001) surface.[29]

Kinetics and Mechanism of Gr Intercalation and Etching. To obtain more quantitative information on the CeO_x-mediated intercalation mechanism and kinetics, the extent of intercalation at different temperatures has been followed by AES. In Figure 3, the fractional Gr coverage and the O_{KLL}/Ru_{MNV} ratio during annealing in O_2 in the 600−725 K range are plotted in the same way as in Figure 1f (both heating and cooling was performed in molecular oxygen). At the lowest temperature used (604 K), the intercalation of oxygen (increase of the O_{KLL}/Ru_{MNV} ratio) is clearly decoupled from the etching of Gr (decrease of the fractional Gr coverage). At higher temperatures, both intercalation and etching of Gr are active.

An additional question arises from the observed increase of the O_{KLL}/Ru_{MNV} saturation ratio with decreasing intercalation temperature in Figure 3. This effect can be explained by considering both intercalation and etching of graphene, since etched Gr areas adopt a $p(2 \times 2)$ structure,[22,42] while intercalated areas have a $p(2 \times 1)$−O structure, and the latter is capable of storing twice as much oxygen compared to the etched Gr areas (see Figure 2). With the use of STM and AES, the O_{KLL}/Ru_{MNV} ratio of the $p(2 \times 2)$−O/Ru(0001) surface was determined to be 0.17 ± 0.01. Consequently, the $p(2 \times 1)$−O structure should correspond to an O_{KLL}/Ru_{MNV} ratio of ~0.34. Therefore, at low temperature (604 K), etching of Gr is negligible and the O_{KLL}/Ru_{MNV} ratio approaches the value corresponding to a fully intercalated Gr with a $p(2 \times 1)$−O structure underneath. At higher temperatures, etching of Gr is more pronounced, and the highest temperature of 721 K, the value is near that for $p(2 \times 2)$−O/Ru(0001).

The temperature-dependent studies of Figure 3 allow us to determine the apparent activation energy (E_a) for intercalation and etching. In Figure 4, an Arrhenius plot for a constant extent of intercalation

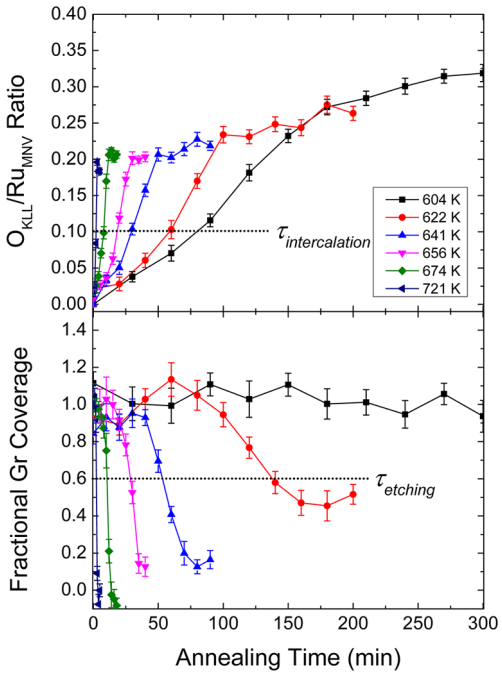

Figure 3. Time-dependent studies of oxygen intercalation and Gr etching for temperatures in the 600−725 K range. The oxygen concentration was determined by the ratio of O_{KLL}/Ru_{MNV} transitions. The fractional Gr coverage was determined from the asymmetry of the 272−273 eV AES peak (overlapping C_{KLL} and Ru_{MNN} transitions, see Figure S2). The highlighted $\tau_{intercalation}$ and $\tau_{etching}$ intercepts were used for further data analysis.

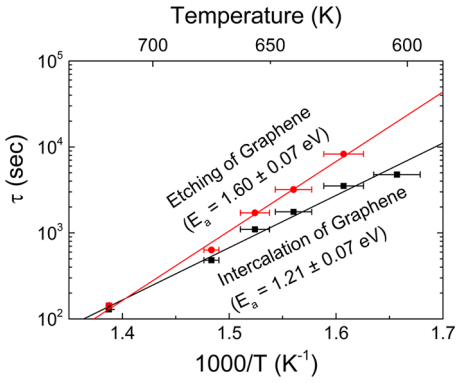

Figure 4. Apparent activation energy for Gr intercalation and etching, determined for a constant intercalation (O_{KLL}/Ru_{MNV} = 0.1 AES peak ratio) or etching (fractional Gr coverage of 0.6) extent from kinetic studies shown in Figure 3. The temperature error bars are obtained as a standard deviation from the averaged time-dependent temperature during the annealing experiments.

(O_{KLL}/Ru_{MNV} = 0.1, $\tau_{intercalation}$ in Figure 3) and etching (fractional Gr coverage = 0.6, $\tau_{etching}$ in Figure 3) is shown. The apparent E_a for Gr intercalation is determined to be 1.21 ± 0.07 eV, while for the etching of Gr, a value of 1.60 ± 0.07 eV is obtained. The latter value is higher than the E_a reported for etching of Gr flakes on Ru(0001).[24] In both cases, the error margin was determined from the standard deviation of the linear regression fitting. For Gr etching, the longest $\tau_{etching}$ at the lowest temperature of 604 K has not been determined due to its extended length, but the linear extrapolation in Figure 4 predicts that this amount of Gr etching will be reached after ~330 min of annealing in oxygen.

During imaging of CeO_x clusters with STM, frequent tip changes induced by the interaction with the clusters have been observed (see Figure S3). In addition, a strong interaction of the STM tip with the CeO_x clusters for very small values of bias voltage (tens of mV) has been noticed, when the STM tip virtually swept away the clusters from the imaged area (see Figure S4). We utilized this effect, which is indicative of weak cluster binding to the Gr substrate, to image the structure of Gr underneath the clusters during the intercalation. In Figure 5a, a partially intercalated surface was imaged with V_{sample} = −1.6 V. Then, all clusters were displaced from the area of interest (by using V_{sample} = +22 mV). Scanning the same area again with the initial voltage (V_{sample} = −1.6 V, Figure 5b) revealed the presence of a small hole (diameter of ~2 nm) underneath some clusters. The nanohole is not present underneath all clusters (clusters with a hole underneath are highlighted with white arrows, other clusters with gray arrows in Figure 5).

When the STM tip interacted with CeO_x clusters on Gr/Ru(0001), contrast inversion of Gr and intercalated Gr in the STM images has been frequently observed (see Figure S3). However, CeO_x clusters were always imaged bright, irrespective of the STM tip termination. As reported previously, the appearance of Gr in STM is strongly dependent on the imaging conditions.[14] We also find that the appearance of Gr (both intercalated and nonintercalated) can be also strongly dependent on the composition of the STM tip apex.

The results presented in Figures 1−5 demonstrate that the mechanism of oxygen intercalation *via* CeO_x clusters on a full Gr layer on Ru(0001) differs from that in previous studies of oxygen intercalation on Gr flakes on Ru(0001). For intercalation of Gr partially covering the Ru(0001) surface, oxygen molecules dissociate on exposed metal areas and diffuse to the graphene edge. With the use of low-energy electron microscopy, Sutter *et al.*[24] determined E_a for oxygen intercalation to be 0.38 ± 0.05 eV, and for Gr etching 1.1 ± 0.1 eV. Since the E_a for intercalation was much smaller than that for diffusion of oxygen vacancies on the $p(2 \times 2)$−O/Ru(0001) surface[43] (E_a = 0.7 eV), the reaction-limited step was assigned to the decoupling of Gr from the Ru(0001) substrate.[24] In the case of a full Gr layer, the mechanism of intercalation has to be different from that on Gr flakes partially covering the Ru(0001) surface. There are no exposed metal areas where oxygen molecules could dissociate and the full Gr layer protects the Ru(0001) substrate against oxidation, as found in previous studies.[27,30] This has been verified for an O_2 pressure of 1×10^{-7} Torr used in this study.

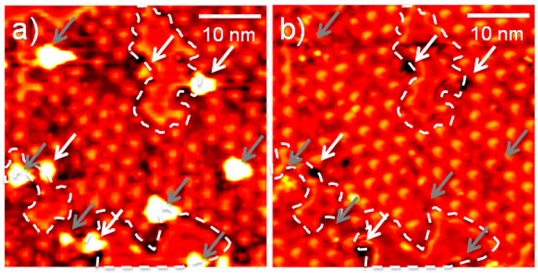

Figure 5. Structure of Gr underneath CeO_x clusters after O_2 intercalation at 604 K for 40 min. The STM image (a) was acquired with $V_{sample} = -1.6$ V and tunneling current $I_{tunnel} = 25$ pA, imaging CeO_x clusters, intercalated Gr areas (highlighted with white, dashed lines) and Gr. Then, the same area was scanned again with $V_{sample} = +22$ mV and the CeO_x clusters were swept away. Panel b shows the same area as in panel a, imaged with identical tunneling conditions. The position of clusters with an open (etched) nanohole underneath is highlighted with white arrows. Clusters without a hole underneath are marked with gray arrows.

With the use of AES, no change of the surface at 641 K for at least 70 min of annealing in O_2 has been detected (see Figure S5d), and for the lower temperature of 604 K, no uptake of oxygen or etching of Gr for exposures exceeding 300 min could be observed (data not shown). On the other hand, with 0.05 ML CeO_x present, a full saturation of the oxygen signal is observed during the time interval in Figure 3. A recent study of Si intercalation on Gr/Ru(0001) has demonstrated the role of point defects in the intercalation process of Si.[44] For gases, the situation appears to be different and Gr with a large number of point defects can still effectively protect the metal substrate against oxidation (see Figure S5). Since other pathways are excluded, the rapid intercalation of oxygen shown in Figure 3 has to be linked to the presence of CeO_x clusters.

Next, we demonstrate that intercalation of oxygen *via* CeO_x clusters can be seen as a two-step process, consisting of the opening of an intercalation gateway underneath the CeO_x clusters, followed by a spillover of oxygen from the clusters to the Ru(0001) substrate. During intercalation of oxygen, we always observed intercalated areas right next to the CeO_x clusters, although not all clusters were involved in the intercalation process (see Figure 1b). The difference between clusters active in intercalation, and the ones that are not, is shown in Figure 5. Here, clusters were displaced by the STM tip from the imaged area, and nanoholes underneath some of the clusters were observed (see white arrows in Figure 5). These nanoholes are smaller than the size of CeO_x clusters, even if the lateral size of the clusters appears generally exaggerated in STM due to a convolution effect with the STM tip. Figure 5 points to the fact that a hole in Gr is necessary to deliver oxygen from the ceria clusters to the Ru substrate, in agreement with previous studies where defects in Gr are required for intercalation.[44,45] As mentioned, the nanoholes are smaller than the CeO_x clusters, or of a similar size. If they were larger than the clusters and the role of CeO_x clusters were merely the formation of a hole in Gr, exposing the Ru(0001) substrate, the same E_a of oxygen intercalation as reported on Gr flakes should be obtained. It is thus proposed that the opening of a hole in Gr between CeO_x and Ru(0001) involves the etching of Gr at the defect site, which is underneath the cluster, through the release of lattice oxygen from the CeO_x cluster and the oxidation of Gr carbon atoms to CO/CO_2. The etching of nanoscale holes in suspended, single-layer Gr by metal particles (Cr, Ti, Pd, Ni, Al) was reported previously by Novoselov *et al.*,[46] and the importance of oxidized layer on the metal was supported by the absence of etching in case of Au nanoparticles. The produced CO/CO_2 molecules can either desorb into the vacuum or get trapped underneath the Gr film. The latter is consistent with the small bright protrusions seen in Figure 2b, which have a high mobility even at RT. Not all clusters have holes underneath; but when clusters are removed, the holes are always found next to intercalated areas.

Once the hole in Gr is opened, the intercalation mechanism involves the spillover of oxygen from CeO_x clusters onto the Ru(0001) substrate. Spillover is generally defined as the indirect adsorption on a support surface (in our case Ru(0001) fully covered with Gr) under conditions, where the direct adsorption is unfavorable.[47] Here, the situation is more complex, because the lattice oxygen in the CeO_x clusters is likely also involved in the process.[1]

The spillover of oxygen between CeO_x nanoparticles and the Ru(0001) metal is further supported by the apparent $E_a = 1.21 \pm 0.07$ eV determined for Gr intercalation in the presence of CeO_x clusters. Since this value is dissimilar to the previously determined $E_a = 0.38$ eV for intercalation on Gr flakes on Ru(0001),[24] and because the full Gr layer on Ru(0001) inhibits intercalation of oxygen (Figure S5), the mechanism of oxygen intercalation observed here can be clearly linked to the CeO_x nanoparticles. While we are unable to conclusively pinpoint the nature of the rate limiting step in the intercalation mechanism, we speculate that the observed apparent E_a reflects the energy required to remove the O atom from the CeO_x nanoparticles. This argument is supported by prior DFT studies, demonstrating that for a small $Ce_{40}O_{80}$ particle, the energy of V_O formation is 0.8−1.2 eV,[48,49] which is much smaller than that on a regular $CeO_2(111)$ slab ($E_a = 2.25$ eV).[49] Despite the uncertainties of the computational studies in the correct determination of E_a on ceria-based systems, the calculated values of E_a for reduction of ceria nanoparticles are in good agreement with the E_a for intercalation measured here.

Oxygen Release from the Intercalated Gr Layer. For Gr flakes, intercalation of oxygen was reported to be reversible by annealing in vacuum.[24,26,28] This was also investigated here for the full Gr layer on Ru(0001) with

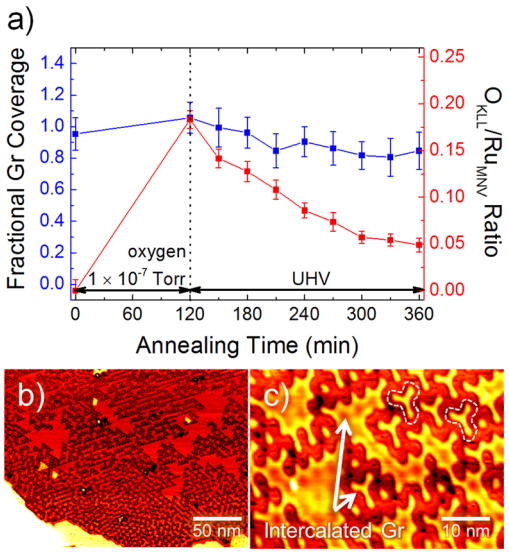

Figure 6. (a) The amount of intercalated oxygen underneath 0.05 ML CeO_x−Gr/Ru(0001) as a function of annealing time. The plot shows the fractional coverage of Gr and the coverage of oxygen during annealing in molecular oxygen at 609 K (intercalation) and in UHV at 604 K (oxygen release). (b) Large-scale STM image recorded from the surface after t = 360 min (corresponding to the last point in panel a), plotted with an inverted contrast (clusters are dark). (c) Zoom-in STM image showing the remaining areas of intercalated oxygen atoms, forming ordered triangular structures. The smallest intercalated areas consist of three intercalated Gr atop regions, forming Y-shaped structures (two of them are highlighted with dashed lines). STM scanning conditions: V_{sample} = −1.6 V, I_{tunnel} = 100 pA.

a coverage of 0.05 ML CeO_x clusters. The sample was annealed at 609 K in O_2 for 120 min, and after storage of a sufficiently large amount of oxygen (58% of the saturation value, see Figure 3), the sample was annealed at 604 K in UHV. Subsequently, the Gr coverage and the amount of intercalated oxygen has been monitored by AES (Figure 6a). After 240 min of annealing in UHV (total time: 360 min in Figure 6a), most of the intercalated oxygen has been released (from 58% to 15% of oxygen saturation value). Further annealing at 604 K did not result in a significant decrease of the O_{KLL}/Ru_{MNV} signal. STM images acquired after the oxygen release revealed the formation of ordered structures formed by the remaining intercalated oxygen underneath the Gr layer (Figure 6b). The zoom-in image in Figure 6c shows that these ordered, intercalated oxygen patterns are formed by building blocks composed of 3, 6, and 10 atop intercalated regions of the Gr cell (we recall that the "(25 × 25) Gr on (23 × 23) Ru" model[13] contains four atop regions per unit cell, corresponding to the weakest bonding between Gr and the Ru substrate, see inset in Figure 1a). The smallest intercalated structures in Figure 6b,c feature a "Y-shape" (two of them are highlighted with dashed lines in Figure 6c), while the larger ones preferentially form triangular-shaped structures. Similar structures have been reported previously for intercalated Si on Gr/Ru(0001).[44] While we were unable to image the

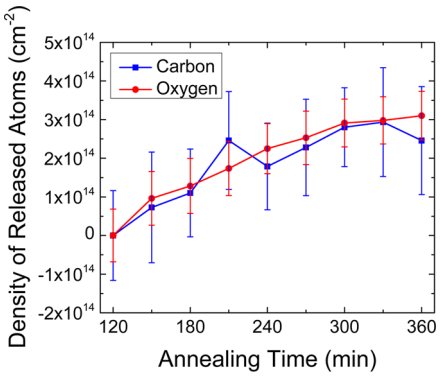

Figure 7. Atomic density of released oxygen and carbon atoms during annealing of the intercalated Gr in vacuum (the time region corresponds to 120−360 min shown in Figure 6a).

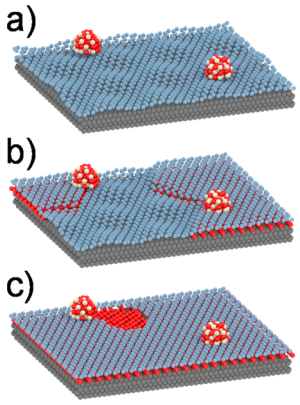

Figure 8. Schematics summarizing the major findings of this study. In the presence of easily reducible CeO_x clusters on the Gr surface (a), Ru(0001) can be readily oxidized *via* intercalation (b), eventually leading to a fully intercalated Gr with oxygen forming a $p(2 \times 1)$ structure underneath. Since intercalated oxygen can attack Gr and etch the film *via* formation of CO, the Gr with CeO_x clusters is less stable and the rate of etching is much higher compared to the bare Gr (c). In the absence of CeO_x clusters, Gr can protect the Ru(0001) substrate against oxidation.

arrangement of oxygen underneath the smallest structures containing three intercalated atop regions, we could confirm the presence of the $p(2 \times 1)$-O intercalated structure underneath the second smallest arrangement comprising 6 Gr atop regions (see Figure S3a−c). While we observe a significant decrease of the oxygen signal during UHV annealing in Figure 6a, there is also a small decrease in the fractional Gr coverage.

Since the density of carbon atoms in Gr/Ru(0001) (1.24×10^{15} atoms/cm^2) and the density of Ru atoms on the Ru(0001) surface (1.57×10^{15} atoms/cm^2) are known, we are able to quantify the ratio of released O atoms to lost C atoms as shown in Figure 6a. A reference measurement of the $p(2 \times 2)$−O/Ru(0001) surface, which has O atoms of 1/4 of the density of Ru(0001) surface atoms, gives a O_{KLL}/Ru_{MNV} ratio of 0.17 ± 0.01 as discussed in the previous section. Using these quantified reference points, the 120−360 min region of Figure 6a is replotted in Figure 7 in the form

of the number of released C and O atoms. The results show a nice 1:1 correspondence between released C and O atoms suggesting that all released O atoms are utilized in Gr etching *via* CO formation. Previous studies on Gr flakes reported that the temperature necessary to desorb intercalated oxygen is much lower (~650 K)[24] than that for the oxygen desorption from the Ru(0001) surface.[28] However, these studies did not exclude the possibility that this lower desorption temperature is caused by reaction of adsorbed oxygen with carbon atoms, resulting in the etching of graphene.[26,28] Moreover, Starodub *et al.*[25] reported that intercalated oxygen can directly attack graphene at a fast rate at temperatures as low as 720 K. Our experiments could also explain the apparent release of intercalated oxygen from Gr flakes during annealing in UHV, starting at the perimeter of the flakes and recoupling the Gr to the Ru(0001) substrate as observed previously.[25]

CONCLUSIONS

We have prepared CeO_x nanoclusters (~3 nm diameter, 1−2 ML height) on a continuous Gr layer on Ru(0001) by evaporating Ce metal in a background of O_2 at room temperature as schematically illustrated in Figure 8a. The clusters remain well-dispersed at elevated temperatures (600−725 K) even though some sintering is observed. In the presence of O_2, the clusters promote the intercalation of oxygen underneath the Gr layer (Figure 8b). We propose that the mechanism for the intercalation comprises the formation of nanoholes (~2 nm size) in the Gr layer directly below the CeO_x nanoclusters, oxygen atom release from the CeO_x clusters, their spillover onto the Ru(0001) metal substrate, and the CeO_x reoxidation with gas phase O_2. Measurements of the temperature-dependent kinetics of the intercalation yield the apparent activation energy of 1.21 eV, which indicates that the rate limiting step is the reduction of the CeO_x nanoclusters. We further show that the release of intercalated oxygen from underneath the Gr layer is not reversible and that annealing in vacuum leads to its reaction with the Gr layer (Figure 8c) and to the formation of CO, which desorbs from the surface. This process is a clear demonstration of the oxygen storage-release capacity ability of CeO_x nanoclusters.

METHODS

All experiments have been carried out in a UHV system with a base pressure below 1×10^{-10} Torr. STM images were obtained using a commercial Omicron variable temperature STM operated at RT in constant current mode and using electrochemically etched W tips. Acquired images were processed by ImageJ software.[50] The processing included background subtraction and noise removal from frequency domain images. Distortion of the STM images was removed using algorithms described in ref 51. The relative concentration of Gr was determined by AES (PerkinElmer) analysis using the ratio of negative to positive excursions of the overlapping Ru_{MNN} (273 eV) and C_{KLL} (272 eV) peaks in $dN(E)/dE$ spectra (see Figure S2).[37,38] Relative oxygen concentration was determined with respect to the Ru_{MNV} (231 eV) peak (unaffected by the presence of graphitic carbon).[37,38] Error bars were determined from the flat regions of the AES spectra.

The Ru(0001) sample (Princeton Scientific Corp.) was mounted on a Ta Omicron sample plate using a thin Ta foil, and heated using a pyrolytic boron nitride (PBN) heater on the manipulator, or in a dedicated electron-beam annealing stage. The temperature for e-beam annealing was measured with an optical pyrometer. On the PBN heating stage, heating was performed using a constant heating power, and the temperature was later calibrated by spot-welding a thermocouple (type K) directly onto the Ru(0001) single crystal. Clean Ru(0001) was prepared by repeated cycles of Ne^+ ion sputtering at 300 K, oxidation in 1×10^{-7} Torr O_2 at 850 K and flash-annealing in UHV above 1600 K. A clean surface was verified by sharp 1×1 spots in LEED and no detectable impurities in AES.

Gr was grown by chemical vapor deposition of ethylene (C_2H_4) at 1100 K for 30 min using a custom built tubular doser with a 3.07 μm pinhole and 8 Torr backing pressure.

Ce (Alfa Aesar, 99.9%) was deposited from a Ta crucible with a high temperature effusion-cell (CreaTec GmbH). The deposition rate was calibrated with a water-cooled quartz crystal microbalance (Inficon) and AES. One ML is defined with respect to the number of C atoms in Gr/Ru(0001), 1.24×10^{15} atoms/cm^2, based on the model presented in ref 13. Oxygen was dosed using a high-precision leak valve, and pressures were measured with a Bayard-Alpert ion gauge. A fixed value of oxygen pressure of 1×10^{-7} Torr was used in all experiments.

Conflict of Interest: The authors declare no competing financial interest.

Supporting Information Available: The Supporting Information is available free of charge on the ACS Publications website at DOI: 10.1021/acsnano.5b03987.

STM images of defects in the as-grown Gr/Ru(0001), reference AES spectra of $p(2 \times 2)$−O/Ru(0001) and 0.05 ML CeO_x-Gr/Ru(0001), STM images revealing the contrast inversion of Gr and intercalated Gr areas with different tip apex composition, an STM image demonstrating tip-cluster interactions for imaging at low bias voltages, and STM and AES studies of oxygen intercalation on sputtered Gr/Ru(0001) surfaces with a different number of point defects (PDF).

Acknowledgment. This work was supported by the U.S. Department of Energy, Office of Basic Energy Sciences, Division of Chemical Sciences, Geosciences & Biosciences and performed in EMSL, a national scientific user facility sponsored by the Department of Energy's Office of Biological and Environmental Research and located at Pacific Northwest National Laboratory (PNNL). PNNL is a multiprogram national laboratory operated for DOE by Battelle. F.P.N. acknowledges the award of an Alternate Sponsored Fellowship at PNNL and financial support of the University of Graz. The authors also acknowledge Dr. Rentao Mu for stimulating discussions.

REFERENCES AND NOTES

1. Perkins, C. L.; Henderson, M. A.; Peden, C. H. F.; Herman, G. S. Self-Diffusion in Ceria. *J. Vac. Sci. Technol., A* **2001**, *19*, 1942–1946.
2. Mullins, D. R. The Surface Chemistry of Cerium Oxide. *Surf. Sci. Rep.* **2015**, *70*, 42–85.
3. Paier, J.; Penschke, C.; Sauer, J. Oxygen Defects and Surface Chemistry of Ceria: Quantum Chemical Studies Compared to Experiment. *Chem. Rev.* **2013**, *113*, 3949–3985.
4. Esch, F.; Fabris, S.; Zhou, L.; Montini, T.; Africh, C.; Fornasiero, P.; Comelli, G.; Rosei, R. Electron Localization Determines Defect Formation on Ceria Substrates. *Science* **2005**, *309*, 752–755.
5. Reed, K.; Cormack, A.; Kulkarni, A.; Mayton, M.; Sayle, D.; Klaessig, F.; Stadler, B. Exploring the Properties and

Applications of Nanoceria: Is There Still Plenty of Room at the Bottom? *Environ. Sci.: Nano* **2014**, *1*, 390–405.
6. Lykhach, Y.; Staudt, T.; Lorenz, M. P. A.; Streber, R.; Bayer, A.; Steinruck, H. P.; Libuda, J. Microscopic Insights into Methane Activation and Related Processes on Pt/Ceria Model Catalysts. *ChemPhysChem* **2010**, *11*, 1496–1504.
7. Zafiris, G. S.; Gorte, R. J. Evidence for Low-Temperature Oxygen Migration from Ceria to Rh. *J. Catal.* **1993**, *139*, 561–567.
8. Happel, M.; Mysliveček, J.; Johánek, V.; Dvořák, F.; Stetsovych, O.; Lykhach, Y.; Matolín, V.; Libuda, J. Adsorption Sites, Metal-Support Interactions, and Oxygen Spillover Identified by Vibrational Spectroscopy of Adsorbed CO: A Model Study on Pt/Ceria Catalysts. *J. Catal.* **2012**, *289*, 118–126.
9. Nolan, M. Charge Transfer and Formation of Reduced Ce^{3+} Upon Adsorption of Metal Atoms at the Ceria (110) Surface. *J. Chem. Phys.* **2012**, *136*, 134703.
10. Fan, X.; Zhang, G.; Zhang, F. Multiple Roles of Graphene in Heterogeneous Catalysis. *Chem. Soc. Rev.* **2015**, *44*, 3023–3035.
11. Singh, V.; Joung, D.; Zhai, L.; Das, S.; Khondaker, S. I.; Seal, S. Graphene Based Materials: Past, Present and Future. *Prog. Mater. Sci.* **2011**, *56*, 1178–1271.
12. Hu, H.; Xin, J. H.; Hu, H.; Wang, X.; Kong, Y. Metal-Free Graphene-Based Catalyst—Insight into the Catalytic Activity: A Short Review. *Appl. Catal., A* **2015**, *492*, 1–9.
13. Martoccia, D.; Willmott, P. R.; Brugger, T.; Björck, M.; Günther, S.; Schlepütz, C. M.; Cervellino, A.; Pauli, S. A.; Patterson, B. D.; Marchini, S.; et al. Graphene on Ru(0001): A 25 × 25 Supercell. *Phys. Rev. Lett.* **2008**, *101*, 126102.
14. Marchini, S.; Gunther, S.; Wintterlin, J. Scanning Tunneling Microscopy of Graphene on Ru(0001). *Phys. Rev. B: Condens. Matter Mater. Phys.* **2007**, *76*, 075429.
15. Batzill, M. The Surface Science of Graphene: Metal Interfaces, CVD Synthesis, Nanoribbons, Chemical Modifications, and Defects. *Surf. Sci. Rep.* **2012**, *67*, 83–115.
16. Han, Y.; Engstfeld, A. K.; Behm, R. J.; Evans, J. W. Atomistic Modeling of the Directed-Assembly of Bimetallic Pt-Ru Nanoclusters on Ru(0001)-Supported Monolayer Graphene. *J. Chem. Phys.* **2013**, *138*, 134703.
17. Sutter, E.; Albrecht, P.; Wang, B.; Bocquet, M. L.; Wu, L. J.; Zhu, Y. M.; Sutter, P. Arrays of Ru Nanoclusters with Narrow Size Distribution Templated by Monolayer Graphene on Ru. *Surf. Sci.* **2011**, *605*, 1676–1684.
18. Liao, Q.; Zhang, H. J.; Wu, K.; Li, H. Y.; Bao, S. N.; He, P. Nucleation and Growth of Monodispersed Cobalt Nanoclusters on Graphene Moiré on Ru(0001). *Nanotechnology* **2011**, *22*, 125303.
19. Zhou, Z.; Gao, F.; Goodman, D. W. Deposition of Metal Clusters on Single-Layer Graphene/Ru(0001): Factors that Govern Cluster Growth. *Surf. Sci.* **2010**, *604*, L31–L38.
20. Pan, Y.; Gao, M.; Huang, L.; Liu, F.; Gao, H. J. Directed Self-Assembly of Monodispersed Platinum Nanoclusters on Graphene Moiré Template. *Appl. Phys. Lett.* **2009**, *95*, 093106.
21. Donner, K.; Jakob, P. Structural Properties and Site Specific Interactions of Pt with the Graphene/Ru(0001) Moiré Overlayer. *J. Chem. Phys.* **2009**, *131*, 164701.
22. Jang, W.-J.; Kim, H.; Jeon, J. H.; Yoon, J. K.; Kahng, S.-J. Recovery and Local-Variation of Dirac Cones in Oxygen-Intercalated Graphene on Ru(0001) Studied Using Scanning Tunneling Microscopy and Spectroscopy. *Phys. Chem. Chem. Phys.* **2013**, *15*, 16019–16023.
23. Sutter, P.; Albrecht, P.; Tong, X.; Sutter, E. Mechanical Decoupling of Graphene from Ru(0001) by Interfacial Reaction with Oxygen. *J. Phys. Chem. C* **2013**, *117*, 6320–6324.
24. Sutter, P.; Sadowski, J. T.; Sutter, E. A. Chemistry under Cover: Tuning Metal−Graphene Interaction by Reactive Intercalation. *J. Am. Chem. Soc.* **2010**, *132*, 8175–8179.
25. Starodub, E.; Bartelt, N. C.; McCarty, K. F. Oxidation of Graphene on Metals. *J. Phys. Chem. C* **2010**, *114*, 5134–5140.
26. Zhang, H.; Fu, Q.; Cui, Y.; Tan, D. L.; Bao, X. H. Growth Mechanism of Graphene on Ru(0001) and O_2 Adsorption on the Graphene/Ru(0001) Surface. *J. Phys. Chem. C* **2009**, *113*, 8296–8301.
27. Granas, E.; Knudsen, J.; Schroder, U. A.; Gerber, T.; Busse, C.; Arman, M. A.; Schulte, K.; Andersen, J. N.; Michely, T. Oxygen Intercalation under Graphene on Ir(111): Energetics, Kinetics, and the Role of Graphene Edges. *ACS Nano* **2012**, *6*, 9951–9963.
28. Dong, A.; Fu, Q.; Wei, M.; Liu, Y.; Ning, Y.; Yang, F.; Bluhm, H.; Bao, X. Facile Oxygen Intercalation Between Full Layer Graphene and Ru(0001) under Ambient Conditions. *Surf. Sci.* **2015**, *634*, 37–43.
29. Over, H. Surface Chemistry of Ruthenium Dioxide in Heterogeneous Catalysis and Electrocatalysis: from Fundamental to Applied Research. *Chem. Rev.* **2012**, *112*, 3356–3426.
30. Sutter, E.; Albrecht, P.; Camino, F. E.; Sutter, P. Monolayer Graphene as Ultimate Chemical Passivation Layer for Arbitrarily Shaped Metal Surfaces. *Carbon* **2010**, *48*, 4414–4420.
31. Liao, Q.; Zhang, H. J.; Wu, K.; Li, H. Y.; Bao, S. N.; He, P. Oxidation of Graphene on Ru(0001) Studied by Scanning Tunneling Microscopy. *Appl. Surf. Sci.* **2010**, *257*, 82–86.
32. Sutter, P. W.; Flege, J. I.; Sutter, E. A. Epitaxial Graphene on Ruthenium. *Nat. Mater.* **2008**, *7*, 406–411.
33. Gyamfi, M.; Eelbo, T.; Wasniowska, M.; Wiesendanger, R. Fe Adatoms on Graphene/Ru(0001): Adsorption Site and Local Electronic Properties. *Phys. Rev. B: Condens. Matter Mater. Phys.* **2011**, *84*, 113403.
34. Mullins, D. R.; Radulovic, P. V.; Overbury, S. H. Ordered Cerium Oxide Thin Films Grown on Ru(0001) and Ni(111). *Surf. Sci.* **1999**, *429*, 186–198.
35. Hansen, T. W.; Delariva, A. T.; Challa, S. R.; Datye, A. K. Sintering of Catalytic Nanoparticles: Particle Migration or Ostwald Ripening? *Acc. Chem. Res.* **2013**, *46*, 1720–1730.
36. Madey, T. E.; Albert Engelhardt, H.; Menzel, D. Adsorption of Oxygen and Oxidation of CO on the Ruthenium (001) Surface. *Surf. Sci.* **1975**, *48*, 304–328.
37. Goodman, D. W.; White, J. M. Measurement of Active Carbon on Ruthenium (110): Relevance to Catalytic Methanation. *Surf. Sci.* **1979**, *90*, 201–203.
38. van Staden, M. J.; Roux, J. P. The Superposition of Carbon and Ruthenium Auger Spectra. *Appl. Surf. Sci.* **1990**, *44*, 259–262.
39. Fei, X.; Zhang, L.; Xiao, W.; Chen, H.; Que, Y.; Liu, L.; Yang, K.; Du, S.; Gao, H.-J. Structural and Electronic Properties of Pb- Intercalated Graphene on Ru(0001). *J. Phys. Chem. C* **2015**, *119*, 9839–9844.
40. Hiebel, F.; Mallet, P.; Varchon, F.; Magaud, L.; Veuillen, J. Y. Graphene-Substrate Interaction on 6H-SiC(000−1): A Scanning Tunneling Microscopy Study. *Phys. Rev. B: Condens. Matter Mater. Phys.* **2008**, *78*, 153412.
41. Mu, R.; Fu, Q.; Jin, L.; Yu, L.; Fang, G.; Tan, D.; Bao, X. Visualizing Chemical Reactions Confined under Graphene. *Angew. Chem., Int. Ed.* **2012**, *51*, 4856–4859.
42. Pan, Y.; Cui, Y.; Stiehler, C.; Nilius, N.; Freund, H.-J. Gold Adsorption on CeO_2 Thin Films Grown on Ru(0001). *J. Phys. Chem. C* **2013**, *117*, 21879–21885.
43. Wintterlin, J.; Trost, J.; Renisch, S.; Schuster, R.; Zambelli, T.; Ertl, G. Real-Time STM Observations of Atomic Equilibrium Fluctuations in an Adsorbate System: O/Ru(0001). *Surf. Sci.* **1997**, *394*, 159–169.
44. Li, G.; Zhou, H.; Pan, L.; Zhang, Y.; Huang, L.; Xu, W.; Du, S.; Ouyang, M.; Ferrari, A. C.; Gao, H.-J. Role of Cooperative Interactions in the Intercalation of Heteroatoms between Graphene and a Metal Substrate. *J. Am. Chem. Soc.* **2015**, *137*, 7099–7103.
45. Alfe, D.; Pozzo, M.; Miniussi, E.; Gunther, S.; Lacovig, P.; Lizzit, S.; Larciprete, R.; Burgos, B. S.; Mentes, T. O.; Locatelli, A. Fine Tuning of Graphene-Metal Adhesion by Surface Alloying. *Sci. Rep.* **2013**, *3*, 2430.
46. Ramasse, Q. M.; Zan, R.; Bangert, U.; Boukhvalov, D. W.; Son, Y. W.; Novoselov, K. S. Direct Experimental Evidence of Metal-Mediated Etching of Suspended Graphene. *ACS Nano* **2012**, *6*, 4063–4071.

47. Jiang, P.; Bao, X.; Salmeron, M. Catalytic Reaction Processes Revealed by Scanning Probe Microcopy. *Acc. Chem. Res.* **2015**, *48*, 1524–1531.
48. Migani, A.; Vayssilov, G. N.; Bromley, S. T.; Illas, F.; Neyman, K. M. Greatly Facilitated Oxygen Vacancy Formation in Ceria Nanocrystallites. *Chem. Commun.* **2010**, *46*, 5936–5938.
49. Vayssilov, G. N.; Lykhach, Y.; Migani, A.; Staudt, T.; Petrova, G. P.; Tsud, N.; Skala, T.; Bruix, A.; Illas, F.; Prince, K. C.; et al. Support Nanostructure Boosts Oxygen Transfer to Catalytically Active Platinum Nanoparticles. *Nat. Mater.* **2011**, *10*, 310–315.
50. Schneider, C. A.; Rasband, W. S.; Eliceiri, K. W. NIH Image to ImageJ: 25 Years of Image Analysis. *Nat. Methods* **2012**, *9*, 671–675.
51. Choi, J. I. J.; Mayr-Schmölzer, W.; Mittendorfer, F.; Redinger, J.; Diebold, U.; Schmid, M. The Growth of Ultra-Thin Zirconia Films on $Pd_3Zr(0001)$. *J. Phys.: Condens. Matter* **2014**, *26*, 225003.